



Published in final edited form as:

Cell. 2014 October 23; 159(3): 608–622. doi:10.1016/j.cell.2014.09.047.

Apocalmodulin Itself Promotes Ion Channel Opening and Ca²⁺ Regulation

Paul J. Adams¹, Manu Ben-Johny¹, Ivy E. Dick¹, Takanari Inoue^{2,3}, and David T. Yue^{1,‡}

David T. Yue: dyue@jhmi.edu

¹Calcium Signals Laboratory, Departments of Biomedical Engineering and Neuroscience, Center for Cell Dynamics, The Johns Hopkins University School of Medicine, Ross Building, Room 713, 720 Rutland Avenue, Baltimore, MD 21205, voice: (410) 955-0078, fax: (410) 614-8269

²Department of Cell Biology and Center for Cell Dynamics, The Johns Hopkins University School of Medicine, 855 N. Wolfe Street, Baltimore, MD 21205

³Precursory Research for Embryonic Science and Technology, Japan Science and Technology Agency, 4-1-8 Honcho Kawaguchi, Saitama 332-0012, Japan

SUMMARY

The Ca²⁺-free form of calmodulin (apoCaM) often appears inert, modulating target molecules only upon conversion to its Ca²⁺-bound form. This schema has appeared to govern voltage-gated Ca²⁺ channels, where apoCaM has been considered a dormant Ca²⁺ sensor, associated with channels, but awaiting the binding of Ca²⁺ ions before inhibiting channel opening to provide vital feedback inhibition. Using single-molecule measurements of channels and chemical dimerization to elevate apoCaM, we find that apoCaM binding on its own markedly upregulates opening, rivaling the strongest forms of modulation. Upon Ca²⁺ binding to this CaM, inhibition may simply reverse the initial upregulation. As RNA edited and spliced channel variants show different affinities for apoCaM, the apoCaM-dependent control mechanisms may underlie the functional diversity of these variants and explain an elongation of neuronal action potentials by apoCaM. More broadly, voltage-gated Na channels adopt this same modulatory principle. ApoCaM thus imparts potent and pervasive ion-channel regulation.

© 2014 Elsevier Inc. All rights reserved.

[‡]Correspondence and requests for materials should be addressed to DTY (dyue@jhmi.edu).

AUTHOR CONTRIBUTIONS

Paul Adams performed Ca_v channel experiments and data analysis. Manu Ben-Johny created mutant channels and undertook Nav experiments and analysis. Paul Adams, Manu Ben-Johny, and David Yue developed the single-versus-multiple-CaM model. Manu Ben-Johny analyzed fluorescence imaging data and built the SN DA neuron model. Ivy Dick supported single-channel data acquisition and analysis, and AP analysis. Takanari Inoue helped develop the FKBP and FRB CaM system. Paul Adams, Manu Ben-Johny and David Yue conceived the project, and refined experimental design. Paul Adams and David Yue wrote the paper.

Publisher's Disclaimer: This is a PDF file of an unedited manuscript that has been accepted for publication. As a service to our customers we are providing this early version of the manuscript. The manuscript will undergo copyediting, typesetting, and review of the resulting proof before it is published in its final citable form. Please note that during the production process errors may be discovered which could affect the content, and all legal disclaimers that apply to the journal pertain.

INTRODUCTION

Calmodulin lacking bound Ca^{2+} (apocalmodulin, apoCaM) has often been categorized as less capable of modulating target molecules, compared to calmodulin (CaM) loaded with Ca^{2+} ($\text{Ca}^{2+}/\text{CaM}$) (Alberts et al., 1994). Certainly, there have been exceptions to this premise (Jurado et al., 1999), but CaM regulation of ion channels has seemingly followed the traditional order (Saimi and Kung, 2002). This study argues to the contrary for voltage-gated Ca^{2+} and Na channels.

Among the most salient examples of CaM modulation are those involving L-type ($\text{Ca}_V1.3$) Ca^{2+} channels. These transport molecules serve as a dominant Ca^{2+} entry pathway into pacemaking cardiomyocytes and neurons (Bean, 2007), and figure crucially in rhythmic functions like cardiac pacemaking and motor control involving substantia nigra, the prime neurodegenerative locus in Parkinson's (Chan et al., 2007; Obeso et al., 2008). As these channels convey substantial Ca^{2+} entry in these settings, modulation of $\text{Ca}_V1.3$ is critical for Ca^{2+} signaling and homeostasis in health and disease (Bean, 2007; Chan et al., 2007; Puopolo et al., 2007).

One better-studied form of $\text{Ca}_V1.3$ regulation is their Ca^{2+} -dependent inactivation (CDI) by CaM (Evans and Zamponi, 2006). At first glance, the operation of CDI may now seem simple in coarse outline, at least for the best-studied $\text{Ca}_V1.3$ channel variant (Ben-Johny and Yue, 2014). This 'archetypical' form is distinguished by an IQ CaM-binding domain containing the sequence isoleucine-glutamine-aspartate-tyrosine (IQDY), followed by a stop codon soon after (Figure 1A, variant 0). A single Ca^{2+} -free CaM molecule (apoCaM) first preassociates with sites including the IQ domain (Figure 1B, configuration A), thus becoming a resident, but presumably dormant Ca^{2+} sensor poised for subsequent channel regulation (Bazzazi et al., 2013; Ben-Johny et al., 2013; Erickson et al., 2003; Liu et al., 2010; Pitt et al., 2001). Ca^{2+} binding to this onboard apoCaM then sharply reduces channel open probability (P_O) (Figure 1B, configuration I) (Ben-Johny et al., 2013), furnishing Ca^{2+} negative feedback crucial for Ca^{2+} handling. Channels without apoCaM cannot undergo CDI (Bazzazi et al., 2013; Ben-Johny et al., 2013; Liu et al., 2010).

That said, the full reality of the modulatory landscape is staggering in its complexity, given recent discoveries of a prominent array of RNA-edited and splice variants of $\text{Ca}_V1.3$ (rest of Figure 1A). RNA editing yields different sequences in the IQ element (Huang et al., 2012), and alternative splicing produces channels with conspicuous extensions after the IQ domain (Bock et al., 2011; Hui et al., 1991; Tan et al., 2011; Xu and Lipscombe, 2001). These newly recognized variants actually constitute the bulk of $\text{Ca}_V1.3$ channels in the brain, and they exhibit vast differences in CDI (Bazzazi et al., 2013; Bock et al., 2011; Huang et al., 2012; Tan et al., 2011), projecting this diversity as an extensive but largely unexplored system for tuning Ca^{2+} dynamics. But CDI tuning may only foreshadow a larger mysterious effect—heterologous expression of $\text{Ca}_V1.3$ variants frequently exhibit sharply diminished current densities that seem too prominent to attribute to happenstance (Bazzazi et al., 2013; Bock et al., 2011; Huang et al., 2012; Tan et al., 2011). Could a major unsuspected action of $\text{Ca}_V1.3$ variation be to adjust baseline channel P_O , thereby producing an equally large or greater effect on Ca^{2+} signaling than CDI? Figure 1C cartoons the potential array of channel

behaviors that would then result, where each hypothetical Ca^{2+} current trace portrays the functional profile of an individual variant. Whether such P_{O} effects actually exist across variants, and whether their mechanistic underpinnings relate to CDI—these remain open and difficult questions that cloud the physiology and pharmacological manipulation of $\text{Ca}_v1.3$ variant channels in relation to Ca^{2+} signaling and dysregulation.

Here, we exploit single-molecule and chemical-biological approaches to reveal a simple principle that may unify the spectrum of $\text{Ca}_v1.3$ molecular variants. In particular, we combine chemical-dimerizer-driven step increases in plasmalemmal CaM with simultaneous electrophysiological readouts of channel function (Luik et al., 2008; Spencer et al., 1993; Suh et al., 2006). We thus reveal that the binding of a single apoCaM to channels does considerably more than permit CDI to occur. ApoCaM binding itself also enhances channel opening (P_{O}) by several fold, rivaling the strongest forms of channel modulation (Miriya et al., 2008). RNA editing, alternative splicing, and fluctuating CaM levels thus regulate CDI and baseline P_{O} , acting to variably populate pools of channels lacking or bound to apoCaM.

A key prediction is that elevated CaM should boost $\text{Ca}_v1.3$ opening and prolong neuronal action potentials. Indeed, we explicitly demonstrate this outcome in substantia nigral neurons. More broadly, a recent study reveals notable similarity between the $\text{Ca}^{2+}/\text{CaM}$ regulation of Ca_v channels and that of voltage-gated Na_v channels (Ben-Johny et al., 2014). Here, we generalize this likeness, showing that apoCaM binding to Na_v channels also strongly amplifies P_{O} . Thus, apoCaM imparts a potent and pervasive form of ion-channel regulation, whose implications range as far as the sweep of Ca_v and Na_v superfamilies, and perhaps beyond (Saimi and Kung, 2002).

RESULTS

CaM Modulates Baseline Opening of L-type channels

We first tested whether the baseline P_{O} of certain variant channels is in fact diminished, and whether CaM at all influences this P_{O} . Figure 1D displays the properties of the canonical $\text{Ca}_v1.3$ ‘short’ splice variant ($\text{Ca}_v1.3_s$, Figure 1B variant ‘0’), with the IQ domain translated as amino acids IQDY (as coded by genomic sequence). We used low-noise electrophysiology (Tay et al., 2012) to directly observe single-channel P_{O} , and employed Ba^{2+} as the charge carrier through channels, because Ba^{2+} binds poorly to CaM (Chao et al., 1984). This maneuver would thus preclude entry into configuration *I* (Figure 1B), allowing alterations in baseline P_{O} to be observed apart from CDI. Accordingly, a slow voltage ramp (shown from -50 to $+40$ mV) elicits stochastic openings that reflect near steady-state P_{O} at each voltage. The top rows display stochastic records, where channel closures correspond to the zero-current portions of the trace (on horizontal gray lines), and openings to downward deflections to the open level (slanted gray curves). Averaging many records yields a mean current that can be divided into the open level (slanted gray curve) to furnish the P_{O} versus voltage relation (sigmoidal trace at bottom), averaged over multiple patches.

Thus appraised, we examined the single-molecule properties of a prominently expressed $\text{Ca}_v1.3$ ‘long’ splice variant (variant 5 in Figure 1A), featuring an extended distal carboxy

tail (DCT) as schematized atop Figure 1E. For convenience, we will refer to this variant as $\text{Ca}_v1.3_L$. Scrutiny of the single-trial records and P_O - V relation for this variant indeed reveals a far lower P_O . Interestingly, the presence of a DCT is not required for a diminished P_O , because Figure 1F shows that a common RNA-edited variant within a short-splice configuration (variant 1 in Figure 1A, or $\text{Ca}_v1.3_{S/MQDY}$) also displays attenuated P_O compared to the canonical $\text{Ca}_v1.3_S$. Curiously, both $\text{Ca}_v1.3_L$ and $\text{Ca}_v1.3_{S/MQDY}$ exhibit diminished apoCaM binding affinity (Bazzazi et al., 2013; Liu et al., 2010). Thus, we tested for P_O effects in a man-made variant, where apoCaM affinity has been attenuated by mutations in the carboxy tail of $\text{Ca}_v1.3_S$ ($\text{Ca}_v1.3_{S/TVM-AAA}$, cartooned atop Figure 1G) (Ben-Johny et al., 2013). $\text{Ca}_v1.3_{S/TVM-AAA}$ also exhibits reduced P_O (Figure 1G).

Given this pattern, we tested more directly for the involvement of apoCaM in modulating P_O , by strongly overexpressing recombinant CaM with these same constructs. Perhaps, P_O might be upregulated by apoCaM occupancy of some site, so that overexpressing CaM may boost occupancy by mass action. For the prototypic ‘short’ variant $\text{Ca}_v1.3_S$, no such enhancement of P_O is produced by CaM overexpression (Figure 1H), as if the hypothetical site were already bound to CaM at baseline. By contrast, elevated CaM produces an impressive increase of P_O in all other constructs with diminished apoCaM affinity (Figure 1I–K), where an appreciable fraction of channels might initially lack indwelling CaM.

Single-channel P_O Modulated in Quantized Manner

However, overexpressing recombinant CaM could enhance channel P_O by a multitude of mechanisms besides binding to a channel modulatory site. For example, CaM-dependent modulation of various kinases and phosphatases, or even gene regulation of auxiliary factors could be in play (Bers and Grandi, 2009). To garner further mechanistic constraints, we considered a distinctive feature of an apoCaM-binding model, as diagrammed atop Figure 2A. Here, beyond the configuration *A* described earlier, we explicitly hypothesize a configuration lacking apoCaM at a P_O modulatory site (configuration *E*). In this formulation, channels bound to apoCaM (configuration *A*) would open with a high P_O as exemplified by $\text{Ca}_v1.3_S$ (Figure 1D), and those lacking apoCaM would exhibit low P_O . A hallmark feature of this paradigm is that channel P_O should be quantized, manifesting as a high P_O ‘mode of channel gating’ when apoCaM is bound (Hess et al., 1984), or a low P_O mode when apoCaM is absent. By contrast, many other mechanisms (e.g., multiple phosphorylation sites) could produce a graded spectrum of intermediate effects. These contrasts might be abundantly clear at the single-channel level.

Figure 2A displays twelve sequential single-channel trials of the RNA-editing variant $\text{Ca}_v1.3_{S/MQDY}$ with only endogenous CaM present. Activity was evoked by voltage ramps introduced at 12-second intervals. The activity appears uniformly sparse, as confirmed by the diary plot of average P_O within individual trials (\bar{P}_O , Figure 2B), as well as the single bell-shaped distribution of P_O drawn from a larger set of trials (Figure 2D). These results are consistent with a channel residing almost exclusively within a hypothesized configuration *E*. The corresponding average P_O - V relation (Figure 2C) may thus pertain to channels residing in configuration *E* alone.

By contrast, upon strongly coexpressing recombinant CaM with another Ca_v1.3_{S/MQDY} channel (Figures 2E–H), activity is markedly enhanced in a conspicuously quantized manner. While many trials exhibit a high P_O pattern of gating (Figure 2E, trials 1, 3, 5–8, 10, 12), low P_O trials resembling those without apoCaM overexpression (Figure 2A) are clearly interspersed (Figure 2E, trials 2, 4, 9, 11). This apparent quantization of high and low P_O gating is confirmed by the segregation of P_O into distinct zones in the diary plot (Figure 2F), and by the bimodal distribution of P_O amassed from a large number of trials (Figure 2H). Little intermediate activity can be discerned. These data are thus consistent with channel switching between discrete E and A configurations. By grouping trials into high and low P_O groups with the dashed-line discriminator in Figure 2F, we could estimate separate P_O - V relations for each gating mode (Figure 2G). Notably, the low P_O - V relation (red) is fit by the same function used without elevating apoCaM (Figure 2C), arguing for the invariance of configuration E between conditions. Also notable is the ~seven-fold enhancement of high versus low P_O - V relations, suggesting an enormous effect of apoCaM on channel opening. Parallel experiments with other Ca_v1.3 variant channels (Ca_v1.3_S, Ca_v1.3_L, Ca_v1.3_{S/TVM-AAA}) confirmed similar quantized behavior (Supplemental Figures S1–S2).

ApoCaM Binding to CDI Site Correlates with Enhanced Baseline P_O

The digital manner by which apoCaM enhances baseline P_O fits well with a simple apoCaM binding mechanism (top of Figure 2). Nonetheless, other plausible mechanisms could also elaborate quantized behavior, such as phosphorylation and dephosphorylation at a single site. To begin to discriminate among these possibilities, we noted that a direct CaM binding mechanism for P_O modulation (Figure 3A) would predict a simple Langmuir relation between the peak P_O measured with only endogenous apoCaM present ($P_{CaM/endo}$) and the association constant for apoCaM binding to a presumed P_O modulatory site (K_a). Supplemental Figure S3 yields:

$$P_{CaM/endo} = P_E + (P_A - P_E) \cdot K_a / (K_a + \Lambda) \quad (1)$$

where P_E is the open probability of channels lacking apoCaM (Figure 3A, configuration E), P_A the open probability of channels prebound to apoCaM (configuration A), and $\Lambda \propto [\text{apoCaM}_{\text{bulk}}]^{-1}$.

The challenge with applying tests based on this equation was the unknown identity of the hypothetical apoCaM binding site for P_O modulation, much less the corresponding K_a for various Ca_v1.3 variants. Indeed, atomic structures of Ca²⁺/CaM complexed with carboxy-tail peptides of closely related Ca_v1.2 channels argue for the binding of multiple CaM molecules per tail, each bound CaM imparting a different function (Fallon et al., 2009; Kim et al., 2010). That said, we conjectured that the apoCaM binding site for P_O modulation might be one and the same as the site involved in the CDI process (Figure 1B). Elsewhere, we have previously determined the K_a values for apoCaM binding to the carboxy-tail site relating to CDI, not only for the Ca_v1.3 variants in Figures 1E–H, but also for additional variants whose P_O profiles are characterized in Figure 3C (Bazzazi et al., 2013; Ben-Johny et al., 2013; Liu et al., 2010). Plotting $P_{CaM/endo}$ versus K_a for all of these variants in Figure 3B then tests for the prediction of Equation 1. It is noteworthy how well the data symbols fit

with the Langmuir function (smooth curve) in Figure 3B, an outcome consistent with the binding of one and same apoCaM modulating both P_O and the ability to undergo CDI. For robustness, open probabilities were measured at maximal depolarization for the plot in Figure 3B.

Rapid Plasmalemmal Recruitment of ApoCaM Triggers Dual Modulation of P_O and CDI

Nonetheless, the suggestive correlation in Figure 3B requires compilation of data from several variants, characterized over multiple cells by differing techniques. By contrast, a considerably more direct test would arise if we could abruptly change the free apoCaM concentration at the cytoplasmic face of channels, all while performing electrophysiology within individual cells. The result would be revealing because the evolving values of CDI and P_O thus observed would adhere to a specific moment-to-moment interrelation, if the one-apoCaM mechanism conjectured above were to hold true. This can be seen as follows in Figure 3D. The top subpanel portrays a hypothetical step-like increase in the free apoCaM concentration facing channels. This ‘input’ would drive a scheme in which channel binding to a single apoCaM imparts a shift from configurations E to A , defined such that channels in E are incapable of undergoing CDI and exhibit a low P_O (P_E), whereas those in A demonstrate a robust CDI and a high P_O (P_A) before undergoing CDI. The following linear relation must then hold for a mixed population of channels, such as observed in whole-cell recordings (Supplemental Figure S4),

$$I_{\text{peak}}/I_{\text{max}}=P_E \cdot (1-CDI)^{-1} \quad (2)$$

where I_{peak} is the peak Ca^{2+} before CDI onset; I_{max} is the current amplitude if all channels in a cell were simultaneously open; CDI is the CDI metric defined in Figure 1C; and P_E is the open probability of channels in configuration E ($= 0.051$ from Figure 3C). In this relation, $(1-CDI)^{-1}$ may be considered a linearized CDI metric, starting at one when CDI is absent, and growing larger as CDI intensifies. As well, $I_{\text{peak}}/I_{\text{max}}$ turns out to be the average peak open probability of all channels in a cell before CDI onset, referred to as P_{peak} . That said, the thin black line in the bottom subpanel of Figure 3D explicitly plots Equation 2. Here, a key feature concerns the immutable interrelation between P_{peak} and $(1-CDI)^{-1}$, even during an abrupt increase of apoCaM. Even though apoCaM binding to channels would deviate from equilibrium during such a transition, all P_{peak} versus $(1-CDI)^{-1}$ points would nonetheless reside on the same line (thick black arrow trajectory). This feature arises because each point on the trajectory corresponds to a specific fraction of channels bound to apoCaM, and each fraction enforces a unique pairing of P_{peak} versus $(1-CDI)^{-1}$ values. In this scheme, then, there are no arrangements that fall outside this regime.

By contrast, if the enhancement of baseline P_O were governed by a separate process other than the apoCaM binding that arms channels for CDI, deviation from the linear relation in Figure 3D would likely occur. For concreteness, consider a system where apoCaM binding to one site enables CDI to proceed (Figure 3E, middle subpanel, configurations within magenta zone), but apoCaM binding to an alternative site (yielding configurations in yellow zone) increases baseline P_O before CDI onset, from P_E to P_A . For simplicity, apoCaM binding to these sites is assumed to occur independently, and the steady-state fraction of

peak current remaining after CDI is set to reproduce the experimentally observed CDI in $\text{Ca}_v1.3_S$ (Ben-Johny et al., 2013). If the dissociation constants for apoCaM binding to P_O ($K_{d|P}$) and CDI ($K_{d|CDI}$) sites were equivalent, then the two-CaM scheme would predict the downwardly convex relation between P_{peak} and $(1-CDI)^{-1}$ (Figure 3E, curve *a* in bottom subpanel), contrasting with the linear relation for the one-CaM scheme. However, if $K_{d|CDI}$ were precisely equal to $K_{d|P} \cdot P_E/P_A$, then the two-CaM scheme would still enforce the linear relation in the bottom subpanel of Figure 3E (curve *b*) at steady state, where this line would be identical to that for the one-CaM scheme (Supplemental Figure S4). However, even here, the difference in dissociation constants at the two sites means that the transient response to abrupt changes in apoCaM would deviate from the linear steady-state relation; this outcome is demonstrated by the numerically simulated hysteretic trajectories in Figure 3E (red), where the CDI regulatory site loads at the same rate or faster than the P_O site as marked (Supplemental Figure S4). In sum, this manner of analysis relating to abrupt changes in apoCaM furnishes powerful means to distinguish among differing mechanisms. Likewise, other potential P_O modulatory mechanisms, like channel phosphorylation, would predict analogous deviations from linearity (Equation 2), particularly during abrupt increases in apoCaM.

We therefore exploited chemical-biological step generation of apoCaM concentration at the cytoplasmic face of channels, based on rapamycin-triggered dimerization of cytoplasmic FK506-binding protein (FKBP) and the FKBP–rapamycin-binding protein (FRB) localized to plasmalemma by a signal sequence from Lyn kinase (Lyn-FRB) (Phua et al., 2012). Figure 4A cartoons the layout, where bath-applied rapamycin should sharply increase perimembranous apoCaM, as confirmed by confocal microscopy visualizing the FKBP–CaM moiety (Figure 4B, top). Line-histogram analysis reveals a six-fold increase of perimembranous CaM with $\tau \sim 20$ s (Suh et al., 2006) (Figure 4B, bottom). Hence, coexpressing $\text{Ca}_v1.3$ variants in this context would permit electrophysiological readouts of P_O and CDI during periods of rapidly increasing apoCaM.

The short splice variant of $\text{Ca}_v1.3$ ($\text{Ca}_v1.3_S$) serves as a control (Figure 4C). Because of its high apoCaM affinity at the CDI site, most channels here might already be charged with apoCaM at baseline, such that increasing apoCaM with rapamycin should produce negligible change. The top two rows display diary plots of peak current and CDI measured from Ca^{2+} currents evoked every 20 seconds by 30-mV step depolarizations, with corresponding current waveforms shown below. The baseline P_O of channels is proportional to peak current, which is displayed in a normalized format (I_{peak}/I_O , as defined below) to facilitate averaging across cells. The metric of CDI (CDI) is specified by I/I_{peak} , with these measures also diagrammed below. As expected, augmentation of apoCaM concentration by rapamycin negligibly perturbed either metric.

By contrast, for an RNA-edited variant ($\text{Ca}_v1.3_{S/MQDY}$) with moderate apoCaM affinity, a markedly different outcome arises (Figure 4D). Here, rapamycin-induced CaM enrichment causes a hand-in-hand increase of peak current and CDI, clearly evident in exemplar traces on the bottom. These trends are entirely corroborated by averaged diary plots above (green circles, top and middle rows). Similarly, parallel increases in peak current and CDI were observed for two other variants featuring reduced aggregate apoCaM affinity (Figures 4E,

F), each with distinctive response kinetics to the step increase of apoCaM. As a control, parallel experiments performed without CaM fused to FKBP invariably showed no changes in either peak current or CDI upon application of rapamycin, verifying that the observed effects were due to CaM enrichment and not FKBP itself (Supplemental Figure S5). Also, current densities for variants predicted to lack apoCaM at baseline (Figures 4D–F) were on average smaller than for Ca_v1.3_S (Figure 4C), as would be expected if P_O were diminished without bound apoCaM (Supplemental Figure S5E). Finally, recruiting a CaM mutant unable to bind Ca²⁺ (CaM₁₂₃₄), and using Ba²⁺ as the charge carrier, provided further evidence that apoCaM is in fact responsible for the observed enhancement in P_O (Supplemental Figure S6).

One CaM Augments Baseline P_O and Enables CDI

With these well-behaved transient responses in hand, we undertook mechanistic analysis relating to moment-to-moment plots of P_{peak} versus $(1-CDI)^{-1}$. Figure 5A renders as dark green symbols the data from the exemplar cell in Figure 4D (Ca_v1.3_{S/MQDY}), with explicit labeling of points (i, ii, and iii) corresponding to exemplar currents shown earlier. The only free parameter is I_{max} in Equation 2, which was adjusted only to vertically normalize the data. Accordingly, the observed linearity and correspondence to predicted slope P_E is intrinsic to the data set. Therefore, adherence of these data points, and those from additional cells (pale green symbols), to the one-CaM relation throughout the CaM step is significant. Applying the same analysis to data from the exemplar cell in Figure 4E (Ca_v1.3_L) also demonstrates strict conformity to the same linear relation, even with numerous points drawn from the transient phase of the response (Figure 5B, dark blue symbols). Points from other cells (pale blue symbols) also adhere nicely to the same relation. Data for the exemplar cell relating to still another variant (Figure 4F, Ca_v1.3_{S/1.4DCT}) also reside on the same line (Figure 5C, dark red symbols), and additional cells also conformed to the same line (pale red symbols). Finally, Figure 5D overlays all these data, and those of another variant (gray symbols, Ca_v1.3_S), thus arguing strongly for compliance with a single linear relation. On this basis, we propose the simple one-apoCaM mechanism in Figure 5E, which may unify the diversity of baseline P_O and CDI properties of numerous variants (Figure 1A). RNA-editing and splice variants modulate P_O and CDI over a large range, largely by tuning the affinity of apoCaM binding to channels (in configuration *E*), rather than by specialized molecular mechanisms particular to each variant. Fluctuations in ambient apoCaM could also tune Ca_v1.3 as shown in Figure 5F. Two realms of generalization immediately follow.

Predicted Neuronal Action Potential Elongation

The strong upregulation of Ca_v1.3 channel P_O by apoCaM promises significant consequences, particularly where Ca_v1.3 channels contribute prominently to pacemaking, such as in the substantia nigral neurons modulating movement control (Chan et al., 2007; Christel et al., 2012; Obeso et al., 2008). Importantly, elevated Ca²⁺ in dopaminergic neurons in the substantia nigra pars compacta (SNc) predisposes for neurodegeneration in Parkinson's disease (Bezprovanny, 2009). Ca_v1.3 channels here support the bulk of Ca²⁺ entry (Bean, 2007; Cardozo and Bean, 1995; Chan et al., 2007; Puopolo et al., 2007), and Ca²⁺ channel activity shapes action potential (AP) morphology (Nedergaard, 1999; Puopolo et al., 2007). These neurons express a variety of Ca_v1.3 splice and RNA-edited variants as

shown in Figure 1A (Bock et al., 2011; Huang et al., 2012), and elevating CaM in these cells drives CaM onto low-affinity channel variants by mass action (Bazzazi et al., 2013). Numerical simulations described below predict that apoCaM enhancement of Ca_v1.3 opening should produce telling changes in action-potential morphology, which we tested for experimentally as follows.

SNC dopaminergic neurons were dissected from transgenic mice selectively expressing GFP under the tyrosine hydroxylase (TH) promoter, enabling robust identification via fluorescence (Figure 6A, left subpanel). After culture for 1–7 days, cells maintained typical autonomous pacing at 1.0 ± 0.03 Hz (middle subpanel) and AP morphology (right subpanel) (Chan et al., 2007; Grace and Bunney, 1984; Puopolo et al., 2007). The AP duration at 90% of baseline (APD₉₀) was 7.4 ± 0.03 ms, as expected from prior reports (Puopolo et al., 2007). To predict the effects of apoCaM-driven P_O enhancement on AP morphology, we performed *in silico* simulations with a model (Chan et al., 2007)(Chan et al., 2007)(Chan et al., 2007)(Chan et al., 2007) that closely recapitulated the firing pattern and AP morphology of these cultured neurons (Figure 6B) (Extended Experimental Procedures). Upon increasing the fraction of Ca_v1.3 channels bound to CaM by three-fold, simulated AP waveforms elongate dramatically from the gray baseline trace to the red waveform (Figure 6C). The top subpanel displays raw waveforms, and the bottom subpanel normalizes these responses to facilitate visual comparison of durations. Current-clamp records in cultured neurons confirmed that enhancement of L-type channel P_O by Bay K8644 induced similar AP prolongation, with APD₉₀ increasing from 4.9 ± 0.92 to 11.5 ± 1.55 ms (Figure 6D). The key test came with lentiviral-mediated overexpression of wild-type CaM, yielding a striking increase of APD₉₀ from 7.4 ± 0.03 ms with endogenous CaM, to 24.3 ± 0.40 ms on overexpressing CaM (Figure 6E). Thus, fluctuations of apoCaM could alter AP morphology in substantia nigra and elsewhere in the brain (Bazzazi et al., 2013).

ApoCaM P_O Modulation Extends to Na_v Channels

The marked apoCaM modulation of Ca_v1.3 gave reason to wonder whether this scheme might generalize to other ion channels. In particular, voltage-gated Na channels (Na_v) have recently been shown to exhibit CaM-mediated CDI that appears remarkably similar to that in Ca_v channels (Ben-Johny et al., 2014). Moreover, earlier experiments report that apoCaM binds the carboxy tail of Na_v channels (Herzog et al., 2003), an interaction confirmed in Supplemental Figure S7. Given the extensive role of Na_v channels in fast electrical conduction within brain, heart, and muscle (Hille, 1984), we tested for apoCaM modulatory effects in Na_v channels. As alanine substitutions in the IQ domain of skeletal muscle Na_v1.4 channels have been shown to both reduce CaM binding and decrease current density (Herzog et al., 2003), we undertook direct single-molecule P_O measurements on this particular channel isoform.

To test for apoCaM modulatory effects, we compared the single-channel activity of wild-type Na_v1.4 (which avidly binds apoCaM at baseline) with that of a mutant Na_v1.4_{IQ/AA} exhibiting weakened apoCaM affinity via IQ to AA substitution within the IQ domain (Supplemental Figure S7). Wild-type recombinant Na_v1.4 channels exhibited frequent stochastic openings of millisecond duration (Figure 7A). Normalizing the ensemble average

of many such records (by unitary current i and number of channels N) yields a robust P_O waveform that peaks at 0.5 (Figure 7B). This outcome is confirmed by plots of peak P_O versus step potential (Figure 7C), averaged from multiple patches. By contrast, $\text{Na}_V1.4_{\text{IQ/AA}}$ channels might often lack apoCaM at baseline. Fitting with a mechanism where such channels would be reluctant to open, corresponding single-molecule records display a sparser pattern of activity with briefer openings (Figure 7D). The ensemble average explicitly confirms this impression, yielding a diminutive P_O waveform (Figure 7E) and P_O - V relation (Figure 7F). Still, this reduced opening could be an intrinsic effect of mutation, rather than of lacking apoCaM. To exclude the former possibility, we strongly coexpressed CaM with $\text{Na}_V1.4_{\text{IQ/AA}}$ channels, a maneuver that should restore apoCaM binding via mass action. Reassuringly, corresponding single-molecule records again exhibit robust activity (Figure 7G), and peak P_O is rescued to near wild-type levels (Figures 7H and 7I), confirming a primary action of apoCaM to elevate P_O . These data therefore support conservation of apoCaM modulation of P_O in both Ca_V and Na_V channel superfamilies. As such, like $\text{Ca}_V1.3$, we propose that $\text{Na}_V1.4$ channels have the potential to reside within one of three configurations (Figure 7J): low P_O configuration E lacking apoCaM; high P_O configuration A bound to apoCaM; and low P_O configuration I bound to $\text{Ca}^{2+}/\text{CaM}$. Each configuration may elaborate distinct Na currents upon step depolarization (Figure 7J, bottom subpanels).

DISCUSSION

Apocalmodulin has been traditionally viewed as playing a secondary role to Ca^{2+} /calmodulin for effectuating molecular function (Alberts et al., 1994). More recently, however, there has been growing awareness that apoCaM serves many roles (Jurado et al., 1999). Here, we reveal that apoCaM itself prominently regulates both voltage-gated Ca^{2+} and Na channels. ApoCaM binding to these channels enhances opening severalfold, matching the strongest forms of ion-channel regulation. This effect may unify understanding of a vast array of channel variants and channelopathic mutations that modulate channel affinity for apoCaM. New avenues are thus opened for understanding and manipulating related diseases.

Before turning to broader ramifications, two enabling methodological advances merit attention. First, low-noise single-channel measurements permit direct observation of quantized regulatory phenomena (Figure 2), crucial to deducing mechanism. Second, chemical-dimerizer-based step generation of perimembrane CaM furnishes powerful means to observe CaM-regulatory events in real time within single cells, excluding ambiguities of data drawn from multiple cells and methods. Importantly, a prior strategy for elevating perimembranous CaM requires kinase activation (Yang et al., 2013), potentially complicating discernment of CaM-specific actions. Moreover, our study illustrates the capability of a step generator to resolve biological signal bifurcation upon the binding of a single molecule (apoCaM imparting both an immediate boost in P_O and subsequent CDI); such mechanisms are difficult to prove by customary steady-state methods. Indeed, the overall approach (Figure 3D) mirrors the phase-plane analysis of electronics, highlighting synergy between biological and electrical network analysis (Jack et al., 1975). Biological signal generators and analysis, based not only on perfusable ligands (Spencer et al., 1993)

but on light activation (Hahn and Kuhlman, 2010; Kennedy et al., 2010; Yazawa et al., 2009), may aid future understanding of other signaling systems.

Mechanistic advances for Ca^{2+} channels are threefold. First, we discover that apoCaM binding to Ca^{2+} channels strongly elevates P_O by up to sevenfold, before the onset of CDI. At least twofold increases of peak current were routinely seen in individual cells undergoing enrichment of apoCaM by rapamycin (Figure 4), but this enhancement is likely a lower bound imposed by limitations of apoCaM recruitment via chemical dimerization (Figure 4B). Using modal analysis of single channels (e.g., Figure 2G), sevenfold augmentation of P_O can be directly deduced. Additionally, the quantitative adherence of all variants to a single line in Figure 5D independently supports this sevenfold P_O modulatory range. That said, the extent of P_O regulation by apoCaM rivals the upregulation of L-type Ca^{2+} channels by adrenergic stimulation (Miriayala et al., 2008), the prototypic modulatory system for fight-or-flight responses (Tsien et al., 1986). Second, we unveil an intimate connection between the modulation of P_O and CDI, where the binding of one and the same apoCaM to channels brings not only the ability to undergo CDI as previously reported (Bazzazi et al., 2013; Ben-Johny et al., 2013; Liu et al., 2010), but the aforementioned increase of initial P_O . Intriguingly, the P_O of channels lacking CaM (Figure 5E, configuration *E*) seems equivalent to that of channels that have undergone CDI (configuration *I*); in particular, $P_E \sim P_I \sim 0.051$. This outcome is visually confirmed by the invariance of steady-state current after 300-ms depolarization during rapamycin in Figure 4 (see exemplar traces). CDI may thus represent a relinquishing of the initial apoCaM enhancement of P_O . For reference, configurations *A* and *I* in Figure 5E explicitly correspond to proposed molecular arrangements in a prior publication (respectively, Figures 8b and 8c in Ben-Johny et al. (2013)). Third, the spectrum of P_O and CDI properties of $\text{Ca}_V1.3$ variants (Figure 1A) can now be unified by a single molecular effect—customization of channel binding to apoCaM (Figure 5E). Notably, beyond this specific effect, the properties of variant channels seem largely equivalent once apoCaM becomes bound or unbound. This conclusion is supported by the adherence of all tested variants to a single relation in Figure 5D. One nuance of this unified view may be that the voltage dependence of activation appears subtly different for a variant with an extended distal carboxy tail that lacks apoCaM (Figures 1E, S1E, and S1F).

The biological implications of these mechanisms are considerable. In particular, the apoCaM affinities of many editing and splice variants are such that natural fluctuations in ambient CaM influence the distribution of channels between pools lacking or armed with apoCaM (Bazzazi et al., 2013; Liu et al., 2010). In switching between pools, we now know that P_O and CDI will be coordinately regulated (Figures 5E–5F). Furthermore, variants tune not only the midpoint sensitivity to apoCaM at steady-state, but also the kinetic response to changes in apoCaM (cf., Figures 4D, E, F), a property now discernible via CaM step generation. Indeed, it will be important to explore the sequelae of these distinctive kinetic and steady-state properties on Ca^{2+} homeostasis and dysfunction, given CaM variation in physiological and disease conditions (Bezprovanny, 2009; Black et al., 2004; Bossuyt and Bers, 2013; Chafouleas et al., 1982; Ikeda et al., 2009; Lesnick et al., 2007; Yacoubian et al., 2008). Specifically, given the marked broadening of action potentials in substantia nigral neurons (Figure 6), it is tempting to speculate that elevated apoCaM predisposes for Ca^{2+} -related

neurodegeneration in Parkinson's. Similar modulatory scenarios may pertain throughout the Ca_v1-2 superfamily (Ben-Johny and Yue, 2014), with corresponding biomedical implications. Finally, the mechanisms revealed here (Figures 5E) sharpen distinctions between CaM abnormalities relating to Ca²⁺/CaM versus apoCaM dysfunction; for example, recently reported CaM missense mutations associated with long-QT syndrome are likely to selectively inhibit transitions into configuration *I* of Ca_v channels (in Figure 5E), while allowing normal access to configuration *A* via maintained binding of Ca²⁺-free mutant CaMs (Limpitikul et al., 2014).

The extension of like mechanisms to other ion-channel families holds the broadest implications. Only recently have Na channels been shown to exhibit CaM-mediated CDI with similarity to Ca_v channels (Ben-Johny et al., 2014). This likeness is now significantly generalized by our finding that apoCaM also robustly amplifies *P*_O of Na_v1.4 (Figure 7). This conserved modulation in Na channels then suggests that channelopathic disease mutations (Lossin, 2009; Schroeter et al., 2010), RNA editing (Song et al., 2004), and alternative splicing (Lossin, 2009) could all alter apoCaM binding and thereby *P*_O. The consequences may be extensive, as the Na_v1.1-1.9 superfamily governs excitability in brain, heart, and skeletal muscle (Hille, 1984), and related diseases encompass epilepsy, autism, pathological pain, cardiac arrhythmias, and skeletal muscle myotonias (Lossin, 2009; Schroeter et al., 2010). More broadly, numerous other transport molecules bind apoCaM (Bosanac et al., 2005; Saimi and Kung, 2002; Samso and Wagenknecht, 2002; Vocke et al., 2013; Wen and Levitan, 2002; Xia et al., 1998). Thus, apocalmodulin promises widespread ion-channel regulation whose scope and stature seem likely to proliferate.

EXPERIMENTAL PROCEDURES

Molecular Biology

Ca_v1.3_S and Ca_v1.3_L are identical to previously published rat Ca_v1.3 (AF370009.1) and rat Ca_v1.3 with human long distal carboxy tail (NM000718), respectively (Liu et al., 2010). Ca_v1.3_S editing/splice variants and apoCaM mutations are same as previously published (Bazzazi et al., 2013; Ben-Johny et al., 2013). Lyn-GFP-FRB construct is same as previously published and YFP-FKBP-CaM was generated from YFP-FKBP-PI(4)P5K (Ueno et al., 2011). Standard cloning and PCR-based strategies for generating Ca_v variants and FKBP-CaM clones are detailed in Extended Experimental Procedures.

Whole-cell Electrophysiology

Voltage-clamp and current-clamp whole-cell recording were performed using an Axopatch 200A amplifier. Data were collected and analyzed using custom MATLAB software (Mathworks). Details of recording conditions and recipes for internal and external solutions are specified in Extended Experimental Procedures.

Single-channel Electrophysiology

Single-channel recordings were performed in the on-cell configuration, using established methods from our laboratory (Tay et al., 2012). To reduce noise, patch pipettes were pulled from ultra-thick-walled borosilicate glass (BF200-116-10, Sutter Instruments), and coated

with Sylgard. Recording conditions, data analysis and recipes for internal and external solutions are provided in Extended Experimental Procedures.

Rapamycin Experiments

Whole-cell currents were recorded for 100 s with regular external solution flowing at 2 mL/min. At 100 s, flow of regular solution was stopped, and flow of the same external containing 200 nM rapamycin was started, triggering dimerization of FRB and FKBP tags that then elevated perimembranous CaM. Flow rates were carefully matched between lines prior to experiments.

Confocal Optical Imaging

Fluorescence images were captured at 20-s intervals, before and after bath application of 200-nM rapamycin. Images were recorded with Olympus Fluoview FV300 and Zeiss LSM710 laser scanning confocal microscopes. Images were analyzed using MATLAB and ImageJ. Details of experimental set-up and data analysis are provided in Extended Experimental Procedures.

SNc Computer Simulation

Action potential waveforms for substantia nigra dopaminergic neurons were simulated using MATLAB 2010b (Mathworks) based on published models. Details of the model are included in Extended Experimental Procedures and Supplemental Table 2.

SNc DA Neuron Culture

SNc neurons were isolated from mice expressing GFP under the tyrosine hydroxylase promoter (TH-GFP) (GENSAT; Rockefeller University) (Gong et al., 2003). Experimental procedures and solution recipes included in Extended Experimental Procedures.

Supplementary Material

Refer to Web version on PubMed Central for supplementary material.

Acknowledgments

We thank Hojjat Bazzazi and Philemon Yang for providing some Ca_v1.3 variants, Ca²⁺ Signals Lab members for valuable comments, and Wanjun Yang for technical support. Supported by grants from the NINDS (to D.T.Y.), NHLBI (D.T.Y.), NIMH (M.B.J.), and Parkinson Society Canada (P.J.A.).

References

- Alberts, B.; Bray, D.; Lewis, J.; Raff, M.; Roberts, K.; Watson, JD. *Molecular biology of the cell*. 3. New York & London: Garland Publishing, Inc; 1994.
- Bazzazi H, Ben Johny M, Adams PJ, Soong TW, Yue DT. Continuously tunable Ca²⁺ regulation of RNA-edited Ca_v1.3 channels. *Cell Rep*. 2013; 5:367–377. [PubMed: 24120865]
- Bean BP. Neurophysiology: stressful pacemaking. *Nature*. 2007; 447:1059–1060. [PubMed: 17597746]
- Ben-Johny M, Yang PS, Bazzazi H, Yue DT. Dynamic switching of calmodulin interactions underlies Ca²⁺ regulation of Ca_v1.3 channels. *Nature communications*. 2013; 4:1717.

- Ben-Johny M, Yang PS, Niu J, Yang W, Joshi-Mukherjee R, Yue DT. Conservation of Ca²⁺/calmodulin regulation across Na and Ca²⁺ channels. *Cell*. 2014; 157:1657–1670. [PubMed: 24949975]
- Ben-Johny M, Yue DT. Calmodulin regulation (calmodulation) of voltage-gated calcium channels. *Journal of General Physiology*. 2014; 143:679–692. [PubMed: 24863929]
- Bers DM, Grandi E. Calcium/calmodulin-dependent kinase II regulation of cardiac ion channels. *Journal of cardiovascular pharmacology*. 2009; 54:180–187. [PubMed: 19333131]
- Bezprozvanny I. Calcium signaling and neurodegenerative diseases. *Trends in Molecular Medicine*. 2009; 15:89–100. [PubMed: 19230774]
- Black DJ, Tran QK, Persechini A. Monitoring the total available calmodulin concentration in intact cells over the physiological range in free Ca²⁺ Cell calcium. 2004; 35:415–425. [PubMed: 15003851]
- Bock G, Gebhart M, Scharinger A, Jangsangthong W, Busquet P, Poggiani C, Sartori S, Mangoni ME, Sinnegger-Brauns MJ, Herzig S, et al. Functional properties of a newly identified C-terminal splice variant of Ca_v1.3 L-type Ca²⁺ channels. *The Journal of biological chemistry*. 2011; 286:42736–42748. [PubMed: 21998310]
- Bosanac I, Yamazaki H, Matsu-Ura T, Michikawa T, Mikoshiba K, Ikura M. Crystal structure of the ligand binding suppressor domain of type 1 inositol 1,4,5-trisphosphate receptor. *Mol Cell*. 2005; 17:193–203. [PubMed: 15664189]
- Bossuyt J, Bers DM. Visualizing CaMKII and CaM activity: a paradigm of compartmentalized signaling. *Journal of molecular medicine*. 2013; 91:907–916. [PubMed: 23775230]
- Cardozo DL, Bean BP. Voltage-dependent calcium channels in rat midbrain dopamine neurons: modulation by dopamine and GABAB receptors. *Journal of neurophysiology*. 1995; 74:1137–1148. [PubMed: 7500139]
- Chafouleas JG, Bolton WE, Hidaka H, Boyd AE 3rd, Means AR. Calmodulin and the cell cycle: involvement in regulation of cell-cycle progression. *Cell*. 1982; 28:41–50. [PubMed: 7066986]
- Chan CS, Guzman JN, Ilijic E, Mercer JN, Rick C, Tkatch T, Meredith GE, Surmeier DJ. ‘Rejuvenation’ protects neurons in mouse models of Parkinson’s disease. *Nature*. 2007; 447:1081–1086. [PubMed: 17558391]
- Chao SH, Suzuki Y, Zysk JR, Cheung WY. Activation of calmodulin by various metal cations as a function of ionic radius. *Mol Pharmacol*. 1984; 26:75–82. [PubMed: 6087119]
- Christel CJ, Cardona N, Mesirca P, Herrmann S, Hofmann F, Striessnig J, Ludwig A, Mangoni ME, Lee A. Distinct localization and modulation of Ca_v1.2 and Ca_v1.3 L-type Ca²⁺ channels in mouse sinoatrial node. *The Journal of physiology*. 2012; 590:6327–6342. [PubMed: 23045342]
- Erickson MG, Liang H, Mori MX, Yue DT. FRET two-hybrid mapping reveals function and location of L-type Ca²⁺ channel CaM preassociation. *Neuron*. 2003; 39:97–107. [PubMed: 12848935]
- Evans RM, Zamponi GW. Presynaptic Ca²⁺ channels--integration centers for neuronal signaling pathways. *Trends in neurosciences*. 2006; 29:617–624. [PubMed: 16942804]
- Fallon JL, Baker MR, Xiong L, Loy RE, Yang G, Dirksen RT, Hamilton SL, Quirocho FA. Crystal structure of dimeric cardiac L-type calcium channel regulatory domains bridged by Ca²⁺ calmodulins. *Proceedings of the National Academy of Sciences of the United States of America*. 2009; 106:5135–5140. [PubMed: 19279214]
- Gong S, Zheng C, Doughty ML, Losos K, Didkovsky N, Schambra UB, Nowak NJ, Joyner A, Leblanc G, Hatten ME, et al. A gene expression atlas of the central nervous system based on bacterial artificial chromosomes. *Nature*. 2003; 425:917–925. [PubMed: 14586460]
- Grace AA, Bunney BS. The control of firing pattern in nigral dopamine neurons: single spike firing. *J Neurosci*. 1984; 4:2866–2876. [PubMed: 6150070]
- Hahn KM, Kuhlman B. Hold me tightly LOV. *Nature methods*. 2010; 7:595, 597. [PubMed: 20676078]
- Herzog RI, Liu C, Waxman SG, Cummins TR. Calmodulin binds to the C terminus of sodium channels Na_v1.4 and Na_v1.6 and differentially modulates their functional properties. *J Neurosci*. 2003; 23:8261–8270. [PubMed: 12967988]
- Hess P, Lansman JB, Tsien RW. Different modes of Ca channel gating behaviour favoured by dihydropyridine Ca agonists and antagonists. *Nature*. 1984; 311:538–544. [PubMed: 6207437]

- Hille, B. Ionic channels of excitable membranes. Sunderland, MA: Sinauer Associates; 1984.
- Huang H, Tan BZ, Shen Y, Tao J, Jiang F, Sung YY, Ng CK, Raida M, Kohr G, Higuchi M, et al. RNA editing of the IQ domain in $\text{Ca}_v1.3$ channels modulates their Ca^{2+} -dependent inactivation. *Neuron*. 2012; 73:304–316. [PubMed: 22284185]
- Hui A, Ellinor PT, Krizanova O, Wang JJ, Diebold RJ, Schwartz A. Molecular cloning of multiple subtypes of a novel rat brain isoform of the alpha 1 subunit of the voltage-dependent calcium channel. *Neuron*. 1991; 7:35–44. [PubMed: 1648940]
- Ikeda S, He A, Kong SW, Lu J, Bejar R, Bodyak N, Lee KH, Ma Q, Kang PM, Golub TR, et al. MicroRNA-1 negatively regulates expression of the hypertrophy-associated calmodulin and *Mef2a* genes. *Molecular and cellular biology*. 2009; 29:2193–2204. [PubMed: 19188439]
- Imredy JP, Yue DT. Mechanism of Ca^{2+} -sensitive inactivation of L-type Ca^{2+} channels. *Neuron*. 1994; 12:1301–1318. [PubMed: 8011340]
- Jack, JJB.; Noble, D.; Tsien, RW. Electric current flow in excitable cells. Oxford, England: Clarendon Press; 1975.
- Jurado LA, Chockalingam PS, Jarrett HW. Apocalmodulin. *Physiol Rev*. 1999; 79:661–682. [PubMed: 10390515]
- Kennedy MJ, Hughes RM, Peteya LA, Schwartz JW, Ehlers MD, Tucker CL. Rapid blue-light-mediated induction of protein interactions in living cells. *Nature methods*. 2010; 7:973–975. [PubMed: 21037589]
- Kim EY, Rumpf CH, Van Petegem F, Arant RJ, Findeisen F, Cooley ES, Isacoff EY, Minor DL Jr. Multiple C-terminal tail Ca^{2+} /CaMs regulate $\text{Ca}_v1.2$ function but do not mediate channel dimerization. *The EMBO journal*. 2010; 29:3924–3938. [PubMed: 20953164]
- Lesnick TG, Papapetropoulos S, Mash DC, Ffrench-Mullen J, Shehadeh L, de Andrade M, Henley JR, Rocca WA, Ahlskog JE, Maraganore DM. A genomic pathway approach to a complex disease: axon guidance and Parkinson disease. *PLoS genetics*. 2007; 3:e98. [PubMed: 17571925]
- Limpitkul WB, Dick IE, Joshi-Mukherjee R, Overgaard MT, George AL Jr, Yue DT. Calmodulin mutations associated with long QT syndrome prevent inactivation of cardiac L-type Ca currents and promote proarrhythmic behavior in ventricular myocytes. *Journal of molecular and cellular cardiology*. 2014; 74C:115–124. [PubMed: 24816216]
- Liu X, Yang PS, Yang W, Yue DT. Enzyme-inhibitor-like tuning of Ca^{2+} channel connectivity with calmodulin. *Nature*. 2010; 463:968–972. [PubMed: 20139964]
- Lossin C. A catalog of SCN1A variants. *Brain Dev*. 2009; 31:114–130. [PubMed: 18804930]
- Luiik RM, Wang B, Prakriya M, Wu MM, Lewis RS. Oligomerization of STIM1 couples ER calcium depletion to CRAC channel activation. *Nature*. 2008; 454:538–542. [PubMed: 18596693]
- Miriyala J, Nguyen T, Yue DT, Colecraft HM. Role of $\text{Ca}_v\beta$ subunits, and lack of functional reserve, in protein kinase A modulation of cardiac $\text{Ca}_v1.2$ channels. *Circulation research*. 2008; 102:e54–64. [PubMed: 18356540]
- Nedergaard S. Regulation of action potential size and excitability in substantia nigra compacta neurons: sensitivity to 4-aminopyridine. *Journal of neurophysiology*. 1999; 82:2903–2913. [PubMed: 10601428]
- Obeso JA, Marin C, Rodriguez-Oroz C, Blesa J, Benitez-Temino B, Mena-Segovia J, Rodriguez M, Olanow CW. The basal ganglia in Parkinson's disease: current concepts and unexplained observations. *Annals of neurology*. 2008; 64(Suppl 2):S30–46. [PubMed: 19127584]
- Phua SC, Pohlmeier C, Inoue T. Rapidly relocating molecules between organelles to manipulate small GTPase activity. *ACS chemical biology*. 2012; 7:1950–1955. [PubMed: 22999378]
- Pitt GS, Zuhlke RD, Hudmon A, Schulman H, Reuter H, Tsien RW. Molecular basis of calmodulin tethering and Ca^{2+} -dependent inactivation of L-type Ca^{2+} channels. *The Journal of biological chemistry*. 2001; 276:30794–30802. [PubMed: 11408490]
- Puopolo M, Raviola E, Bean BP. Roles of subthreshold calcium current and sodium current in spontaneous firing of mouse midbrain dopamine neurons. *J Neurosci*. 2007; 27:645–656. [PubMed: 17234596]
- Saimi Y, Kung C. Calmodulin as an ion channel subunit. *Annual review of physiology*. 2002; 64:289–311.

- Samsø M, Wagenknecht T. Apocalmodulin and Ca²⁺-calmodulin bind to neighboring locations on the ryanodine receptor. *The Journal of biological chemistry*. 2002; 277:1349–1353. [PubMed: 11694536]
- Schroeter A, Walzik S, Blechschmidt S, Haufe V, Benndorf K, Zimmer T. Structure and function of splice variants of the cardiac voltage-gated sodium channel Na_v1.5. *Journal of molecular and cellular cardiology*. 2010; 49:16–24. [PubMed: 20398673]
- Song W, Liu Z, Tan J, Nomura Y, Dong K. RNA editing generates tissue-specific sodium channels with distinct gating properties. *The Journal of biological chemistry*. 2004; 279:32554–32561. [PubMed: 15136570]
- Spencer DM, Wandless TJ, Schreiber SL, Crabtree GR. Controlling signal transduction with synthetic ligands. *Science*. 1993; 262:1019–1024. [PubMed: 7694365]
- Suh BC, Inoue T, Meyer T, Hille B. Rapid chemically induced changes of PtdIns(4,5)P₂ gate KCNQ ion channels. *Science*. 2006; 314:1454–1457. [PubMed: 16990515]
- Tan BZ, Jiang F, Tan MY, Yu D, Huang H, Shen Y, Soong TW. Functional characterization of alternative splicing in the C terminus of L-type Ca_v1.3 channels. *The Journal of biological chemistry*. 2011; 286:42725–42735. [PubMed: 21998309]
- Tay LH, Dick IE, Yang W, Mank M, Griesbeck O, Yue DT. Nanodomain Ca²⁺ of Ca²⁺ channels detected by a tethered genetically encoded Ca²⁺ sensor. *Nature communications*. 2012; 3:778.
- Tsien RW, Bean BP, Hess P, Lansman JB, Nilius B, Nowycky MC. Mechanisms of calcium channel modulation by beta-adrenergic agents and dihydropyridine calcium agonists. *Journal of molecular and cellular cardiology*. 1986; 18:691–710. [PubMed: 2427730]
- Ueno T, Falkenburger BH, Pohlmeier C, Inoue T. Triggering actin comets versus membrane ruffles: distinctive effects of phosphoinositides on actin reorganization. *Science signaling*. 2011; 4:ra87. [PubMed: 22169478]
- Vocke K, Dauner K, Hahn A, Ulbrich A, Broecker J, Keller S, Frings S, Mohrlen F. Calmodulin-dependent activation and inactivation of anoctamin calcium-gated chloride channels. *The Journal of general physiology*. 2013; 142:381–404. [PubMed: 24081981]
- Wen H, Levitan IB. Calmodulin is an auxiliary subunit of KCNQ2/3 potassium channels. *J Neurosci*. 2002; 22:7991–8001. [PubMed: 12223552]
- Xia XM, Fakler B, Rivard A, Wayman G, Johnson-Pais T, Keen JE, Ishii T, Hirschberg B, Bond CT, Lutsenko S, et al. Mechanism of calcium gating in small-conductance calcium-activated potassium channels. *Nature*. 1998; 395:503–507. [PubMed: 9774106]
- Xu W, Lipscombe D. Neuronal Ca_v1.3α(1) L-type channels activate at relatively hyperpolarized membrane potentials and are incompletely inhibited by dihydropyridines. *J Neurosci*. 2001; 21:5944–5951. [PubMed: 11487617]
- Yacoubian TA, Cantuti-Castelvetri I, Bouzou B, Asteris G, McLean PJ, Hyman BT, Standaert DG. Transcriptional dysregulation in a transgenic model of Parkinson disease. *Neurobiology of disease*. 2008; 29:515–528. [PubMed: 18191405]
- Yang T, He LL, Chen M, Fang K, Colecraft HM. Bio-inspired voltage-dependent calcium channel blockers. *Nature communications*. 2013; 4:2540.
- Yazawa M, Sadaghiani AM, Hsueh B, Dolmetsch RE. Induction of protein-protein interactions in live cells using light. *Nature biotechnology*. 2009; 27:941–945.

HIGHLIGHTS

- ApoCaM binding to Ca_v1.3 channels boosts channel open probability up to seven fold
- RNA editing and alternative splicing of Ca_v1.3 tunes apoCaM affinity
- One apoCaM boosts both opening and subsequent Ca²⁺-dependent channel inactivation
- ApoCaM modulation of open probability is conserved between Ca_v and Na_v channels

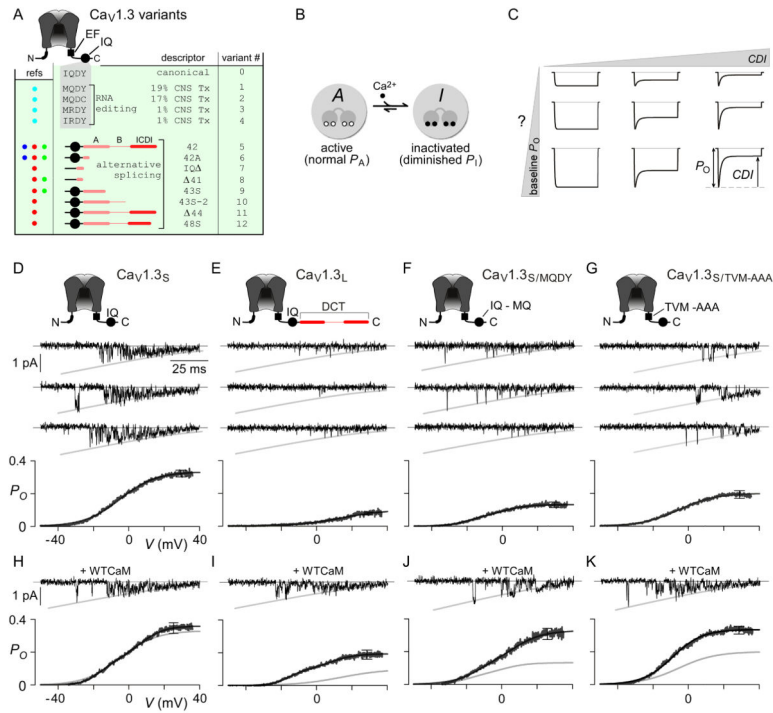


Figure 1. CaM Alters P_O of L-type Channel Variants at Single-Molecule Level

(A) Cav1.3 channel carboxy tail variation by alternative splicing and RNA-editing. Cyan, blue, red, and green symbols correspond respectively to references Huang et al. 2012; Hui et al. 1991; Tan et al. 2011; Bock et al. 2011. (B) Configuration *A* (active), channels (shown as gray circle) bound to apoCaM (shown as two lobes and linker) have high baseline P_O (P_A). Configuration *I* (inactivated), channels bound to Ca^{2+} -CaM have diminished channel P_O (P_I) (Ben-Johny et al., 2013; Imredy and Yue, 1994). (C) Hypothetical fixed and idiosyncratic CDI and baseline P_O profiles for Cav1.3 variants. (D–G) Single-channel analysis of four recombinant Cav1.3 variants transiently expressed in HEK293 cells with only endogenous CaM present. Top subpanels, unitary Ba^{2+} currents during voltage ramp, shown between -50 mV and $+40$ mV (slanted gray lines, GHK fit). Bottom subpanel, average single-channel P_O versus voltage. (H–K) Single-channel records under elevated apoCaM. Light gray line reproduced from corresponding variant above. All averages derived multiple patches ($n = 4-6$). Error bars are \pm SEM throughout. (A,D) Behaviors shown for Cav1.3_S (Extended Experimental Procedures for detailed sequence) in panels A and D were indistinguishable in this regard to those for a closely similar natural splice variant Cav1.3_{42A} (Xu and Lipscombe, 2001) (not shown).

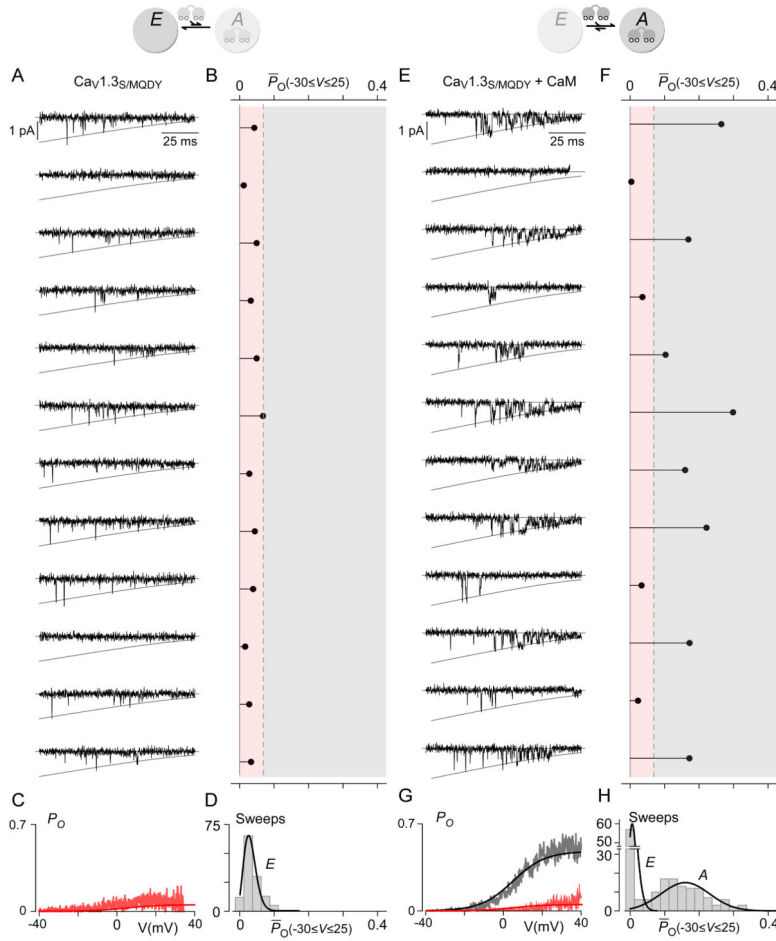


Figure 2. Single-Channel P_O Modulated by CaM in Quantized Manner
 (A) $Ca_v1.3S/MQDY$ in HEK cells with only endogenous CaM present; mainly expected to occupy configuration E (top cartoon). Single-channel Ba^{2+} currents during voltage ramp, shown between -40 and +40 mV, elicited at 12-s intervals. (B) For each current trace in A, average P_O between -30 and +25 mV ($P_O(-30 \leq V \leq 25)$) was calculated. Traces categorized into low P_O (red-shaded) region or high P_O range (gray-shaded). (C) Average P_O at each voltage, calculated separately for traces in low P_O (red) versus high P_O range (gray). In this case, all traces in low P_O group (red). (D) Number of sweeps with $P_O(-30 \leq V \leq 25)$ within indicated P_O ranges. Histogram fits with unimodal distribution ($P > 0.9$) by Hartigan's dip test (Supplemental Extended Procedures). (E-H) Same analysis for $Ca_v1.3S/MQDY$ with CaM overexpression. (H) P_O histogram unlikely to be unimodal ($P < 0.05$, Hartigan's dip test); thus fit by bimodal distribution. See also Supplemental Figures S1 and S2.

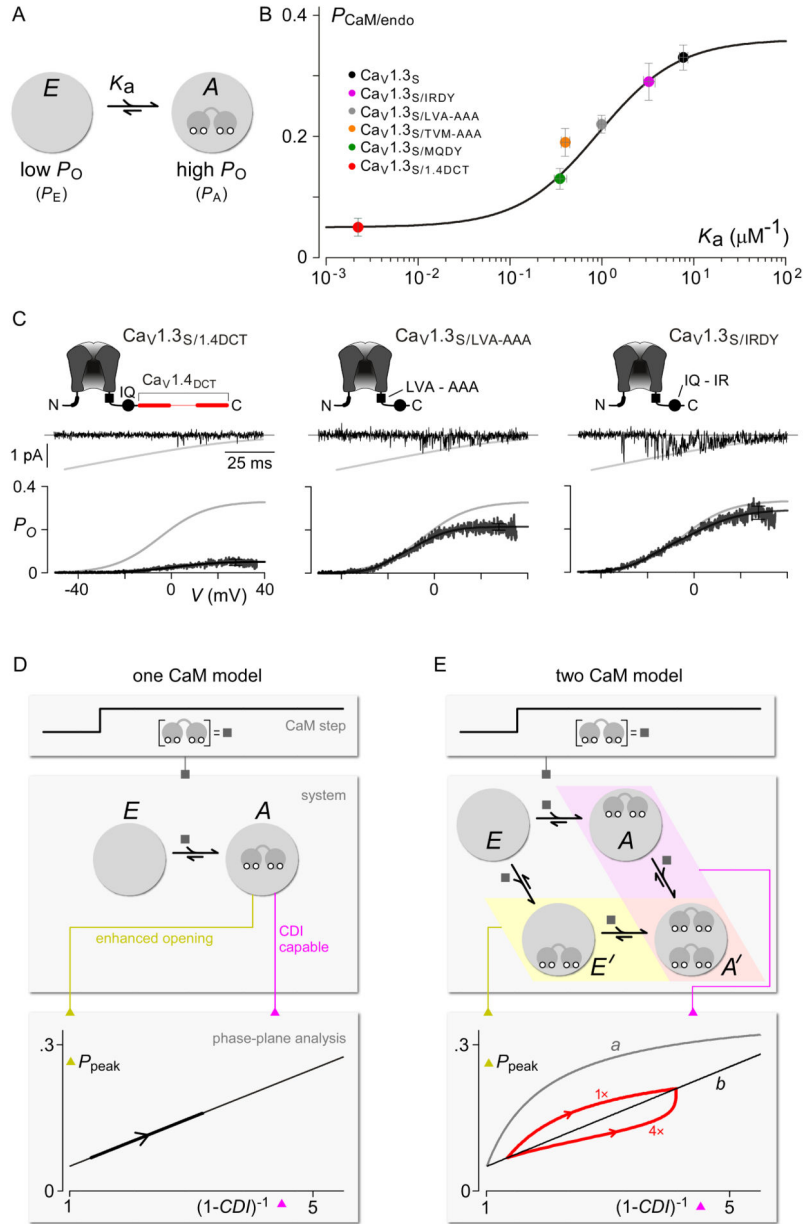


Figure 3. ApoCaM Affinity Tunes P_O

(A) Proposal that channel apoCaM affinity (K_a) specifies equilibrium between configuration E (low P_O) and A (high P_O). (B) Plot of peak P_O obtained with only endogenous CaM present ($P_{CaM/endo}$) versus previously estimated association constants gauged by live-cell FRET between channel carboxy termini and apoCaM (Supplemental Figure S3 and Supplemental Table 1). (C) Average P_O (format as in Figures 1E–1L) for recombinant Cav1.3_S channels with variant carboxy tails yielding reduced apoCaM affinity. Gray lines from basic Cav1.3_S (Figure 1E) for comparison. All averages from multiple patches ($n = 3–6$). (D) Phase-plane signature of single-CaM behavior during CaM transients. (E) Two-CaM behavior during CaM transients, revealed by phase-plane paradigm. See also Supplemental Figure S4.

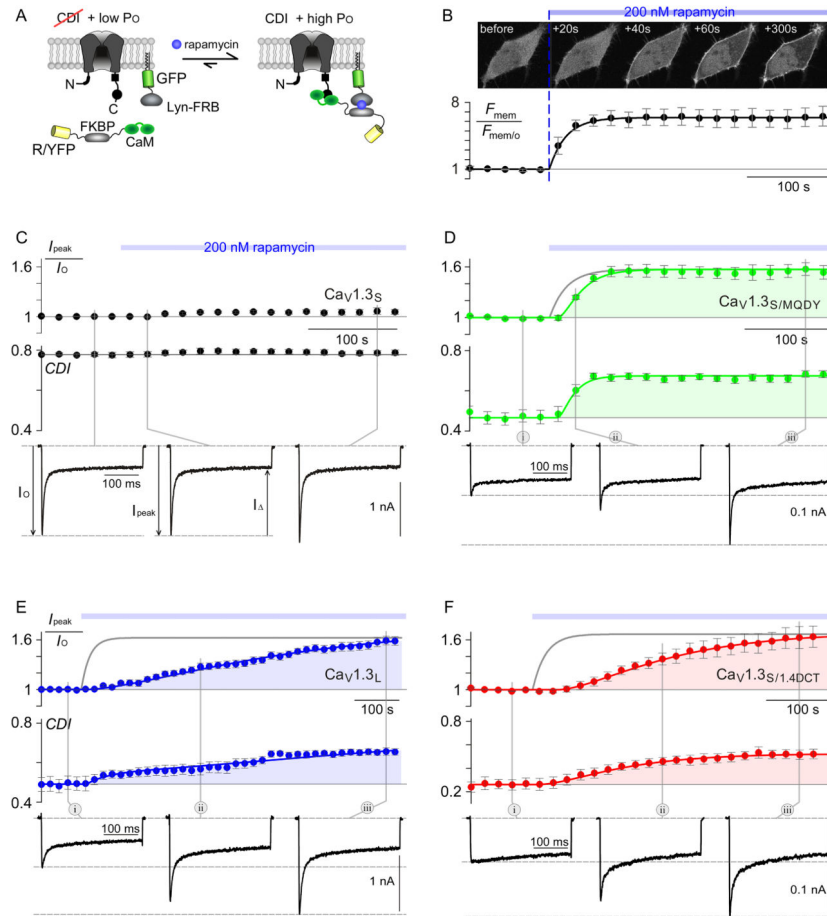


Figure 4. Step Increases in CaM Rapidly Modulate Both Peak Current and CDI
 (A) Recombinant channels in HEK293 cells with both membrane-localized GFP-tagged FRB and cytosolic RFP/YFP-tagged FKBP fused to wild-type CaM. (B) Top, confocal image of RFP/FKBP/CaM translocation to plasma membrane on 200-nM rapamycin perfusion. Bottom, time course of RFP membrane fraction measured every 20 s ($n = 7$ cells). (C) Diary of normalized peak current (top subpanel) and CDI (middle subpanel) from whole-cell Ca^{2+} currents through $\text{Ca}_v1.3_s$ channels, evoked at 20-s intervals by steps to +30 mV from -90 mV holding potential. Corresponding current waveforms below. (D–F) Normalized peak current and CDI for $\text{Ca}_v1.3$ variants with reduced apoCaM affinity. Format as in (C). Gray fit of apoCaM recruitment to plasmalemma from B. All peak current and CDI measures obtained from multiple cells ($n = 4–8$). See also Supplemental Figures S5 and S6.

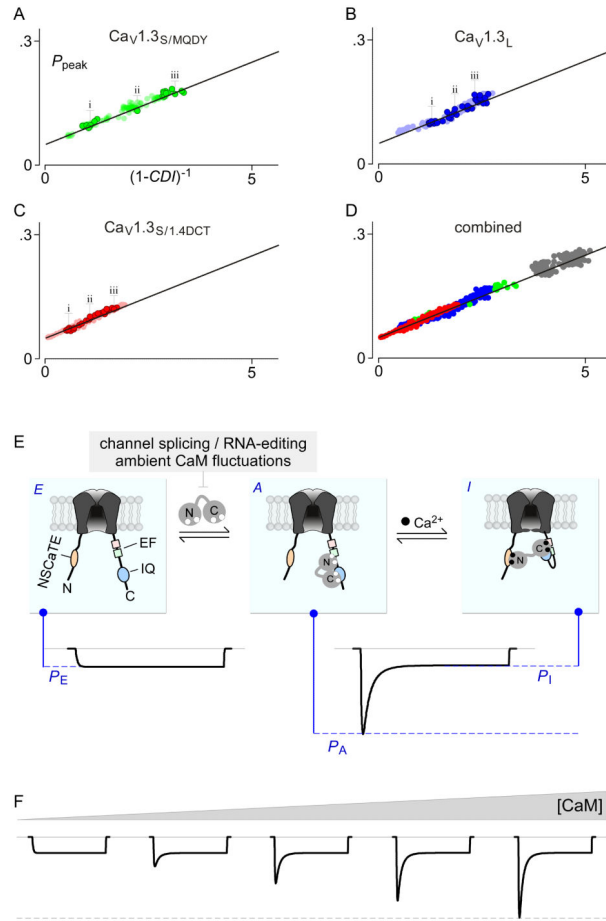


Figure 5. Phase-Plane Analysis Indicates that One CaM Modulates Both P_O and CDI
 (A) Dark green symbols for exemplar cell in Figure 4D ($Ca_v1.3_{S/MQDY}$), with labeled points (i, ii, and iii) corresponding to exemplar currents in Figure 4D. Pale green symbols, data from additional cells expressing $Ca_v1.3_{S/MQDY}$. (B–C) Same analysis for exemplar cells in Figure 4E ($Ca_v1.3_L$, dark blue symbols) and Figure 4F ($Ca_v1.3_{S/1.4DCT}$, dark red symbols), respectively. Pale symbols from additional cells. (D) Data from additional cells for each variant, and for a further canonical $Ca_v1.3_S$ variant (dark gray symbols) ($n = 23$ cells). (E) One-apoCaM mechanism unifies diversity of baseline P_O and CDI properties of $Ca_v1.3$ variants. (F) Simulation of P_O –CDI coordination with free apoCaM concentration for a single $Ca_v1.3$ variant.

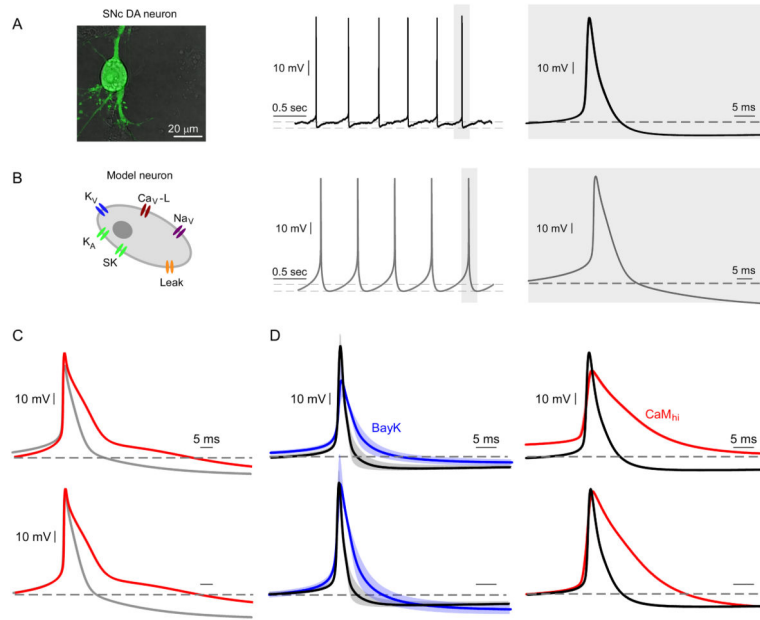


Figure 6. Predicted AP Elongation in Neurons

(A) Confocal image of cultured mouse substantia nigra (pars compacta) dopamine neuron (left subpanel). Middle subpanel, representative current-clamp recording of pacing in a SNc DA neuron in culture. Right subpanel, characteristic AP waveform obtained by averaging ~2100 APs. (B) Quantitative *in silico* model (left subpanel). Numerical simulations of pacing (middle subpanel) and AP morphology (right subpanel). (C) Simulated AP waveforms with fraction of $\text{Ca}_v1.3$ channels bound to apoCaM equal to 0.3 (gray), compared to fraction bound of unity (red). Top subpanel, raw waveforms; bottom subpanel, normalized waveforms. See Extended Experimental Procedures and Supplemental Table 2. (D) Average AP from cultured SNc DA neurons before (black trace), and after applying Bay K8644 ($5\mu\text{M}$) (blue trace) ($n > 620$ APs). (E) AP recorded in SNc DA neurons with only endogenous CaM present (black trace), and with CaM overexpression (red trace) ($n > 800$ APs). All APs measured from $n = 4-5$ cells. SEM shown as shading in panels D and E.

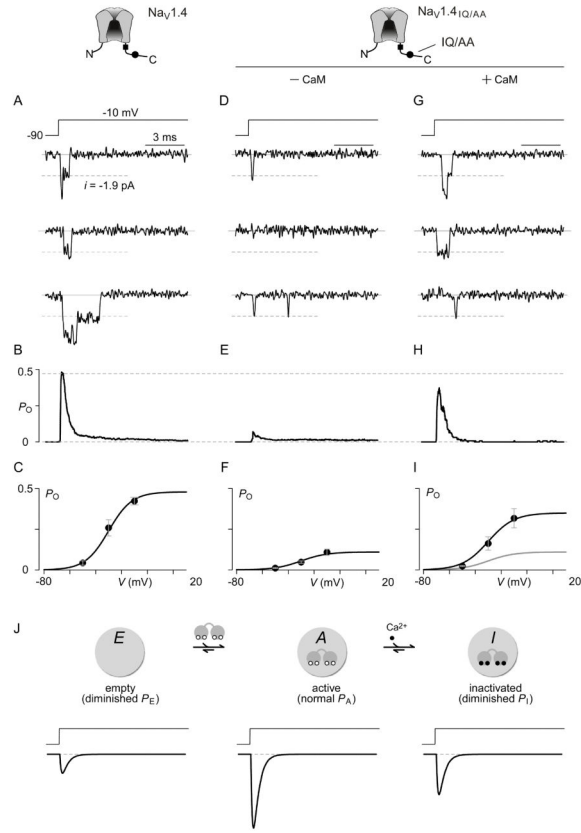


Figure 7. ApoCaM Modulates P_O of Nav1.4 Channels

(A) Single-molecule records of wild-type Nav1.4 channels transiently expressed in HEK cells, with only endogenous CaM. (B) P_O waveform obtained by normalizing ensemble average of >100 records by unitary current i and number of channels N . (C) Plot of peak P_O versus step potential (from -90 mV holding potential), averaged over multiple patches. (D) Single-channel records for Nav1.4 channels containing IQ to AA substitution (Nav1.4_{IQ/AA}). Channels are coexpressed with the CaM chelator, BSCaM_{IQ}, to minimize free CaM levels (Liu et al., 2010). Corresponding P_O waveform (E) and $P_O - V$ relation (F). See also Supplemental Figure S7. (G) Single-channel traces for Nav1.4_{IQ/AA} paired with overexpressed CaM. Corresponding P_O waveform (H) and $P_O - V$ relation (I) both restored to near wild-type levels. $P_O - V$ relations averaged from $n = 5-8$ patches each. Error bars, SEM. (J) Top, proposed Nav configurations with respect to CaM. Bottom, simulated Nav currents for configurations above.